Annals of the Academy of Romanian Scientists
Series on Physics and Chemistry Sciences
ONLINE ISSN 2559-1061 Volume 2, Number 1/2017

ELECTRICAL AND PHOTOELECTRICAL PROPERTIES OF Ge NANOPARTICLES EMBEDDED IN OXIDE

Abstract of Phd. Thesis

Drd. Catalin PALADE[1,2]
Scientific Coordinator: Prof. Magdalena Lidia CIUREA[1,3]

Keywords: magnetron sputtering, rapid thermal annealing, nanocrystals (HfO_2, TiO_2) and Ge quantum dots, memory properties and VIS-NIR photosensing

1. Introduction

In the last two decades, the systems based on nanocrystals (NC) embedded in high-k oxide matrix are intensively investigated due to their potential applications in non-volatile memory devices, photoelectronic sensors, quantum computers, etc. [1-14]. The great interest for NCs/quantum dots (QDs) is motivated by their different electrical, photoelectrical and optical properties in respect to crystalline bulk materials as QDs present the quantum confinement effect, namely the charge carriers (electrons and holes) are confined in the QD volume [2]. By controlling NCs sizes the bandgap is adjusted and therefore the photosensitivity spectral range of the material can be tuned [15]. From the group IV elements, the most used nanostructured materials are Si and Ge, the last one being characterized by a higher quantum confinement effect as the exciton Bohr radius (24.3 nm) is higher compared to Si (4.5 nm). The Ge NCs embedded in oxides present interesting properties that make them suitable for nonvolatile memories and VIS-NIR photodetectors [3, 16, 17]. In the literature, the memory properties of these materials are often reported for MOS like capacitors with a trilayer configuration in which the intermediate layer of Ge NCs embedded in oxide acts as a floating gate layer. The most used oxides are SiO_2 [4-6], HfO_2 [9-13], Al_2O_3 [14, 18, 19], ZrO_2 [7, 8], etc. The advantages of using HfO_2 are given by the high dielectric constant (k = 16 for monoclinic phase and k = 25 for the tetragonal one), low leakage currents and high breakdown voltage which allows memory device downscaling [20]. On the other hand, by embedding Ge NCs in TiO_2, the optical bandgap can be tuned between the Ge NCs bandgap (0.7 eV) and TiO_2 bandgap (3.2 eV for anatase) in function of the Ge content [21]. These results can be achieved by controlling the deposition and the annealing conditions that in turn can essentially influence the electrical and photoelectrical properties.

[1]National Institute of Materials Physics, 405A Atomistilor Street, 077125 Magurele, Romania.
[2] University of Bucharest, Faculty of Physics, 405 Atomistilor Street, 077125 Magurele, Romania.
[3]Academy of Romanian Scientists, 54 Splaiul Independentei, 050094 Bucuresti, Romania.

The aim of the PhD Thesis is to study the electrical (memory) and photoelectrical properties of Ge nanoparticles (NPs) embedded in oxide matrix. The thesis contains three sections from which we extracted two of them for this abstract in which we present the original results only, concerning memory and photoelectrical properties of structures based on Ge NCs embedded in HfO_2 and TiO_2 matrix respectively (the thesis contains an additional section related to the state of the art). In Section 2, the preparation of trilayer MOS-like capacitors based on Ge NCs embedded in HfO_2 is presented. The capacitors were deposited by either magnetron sputtering (MS) or e-beam evaporation (EBE) followed by rapid thermal annealing (RTA) for Ge NCs formation. Then the electrical and memory properties correlated with structure and morphology are studied. In Section 3, the preparation of nanostructured Ge-TiO_2 layers by MS and subsequent RTA is presented and the electrical and photoconduction properties also correlated with structure and morphology are investigated.

2. Study of trilayer MOS-like capacitors based on Ge nanocrystals embedded in HfO_2

The MOS-like capacitor preparation starts with cleaning of Si wafers using Radio Corporation of America (RCA) procedure followed by dipping in diluted HF solution (in water) for native SiO_2 removing. The trilayer MOS like capacitors are deposited by MS and EBE on substrates of p-type Si wafer with 7-14 ohm×cm resistivity. The samples configuration and detailed sizes are presented in Table 1.

Table 1. The samples configuration and detailed sizes

Samples		*Tunnel oxide*	*Floating gate*	*Gate oxide*
A	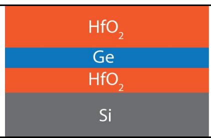	HfO_2, 8 nm	Ge, 3.5 nm	HfO_2, 25 nm
B		HfO_2, 8 nm	Ge- HfO_2, 8 nm	HfO_2, 20 nm
C		–	–	HfO_2, 20 nm

For the sample A, the as-deposited intermediate layer (by MS or EBE) is a continuous Ge layer, while for the sample B it is obtained by co-sputtering of Ge and HfO_2 with Ge:HfO_2 ratio of 50:50. The sample C is a control sample without Ge. The MS deposition was performed in Ar atmosphere using 30 sccm gas flow and 7 mTorr work pressure for all samples A, B and C. In order to form Ge NCs embedded in HfO_2, a RTA process was performed between 600 and 1000 °C in N_2 flow. In samples A deposited by EBE the gate, intermediate and tunnel layers have similar sizes as those deposited by MS (Table 1). The capacitors were configured by Al electrodes thermally deposited on the both sides of samples, having 1 mm^2 area.

The structure and morphology investigations for all samples A were performed. In Figure 2.1 are presented cross-section HRTEM images taken on samples A deposited by MS (A-MS sample) [17]. The as-deposited sample is amorphous (Figure 2.1, a) and the trilayer configuration is clearly evidenced. After the annealing at 600°C (Figure 2.1, b) the whole sample is crystallized (Ge and HfO_2), Ge intermediate layer is visible and positioned at the same place in the trilayer as in the as-deposited samples, while after 850°C RTA the trilayer configuration disappears, Ge being spread by diffusion in the gate HfO_2 layer (Figure 2.1, c).

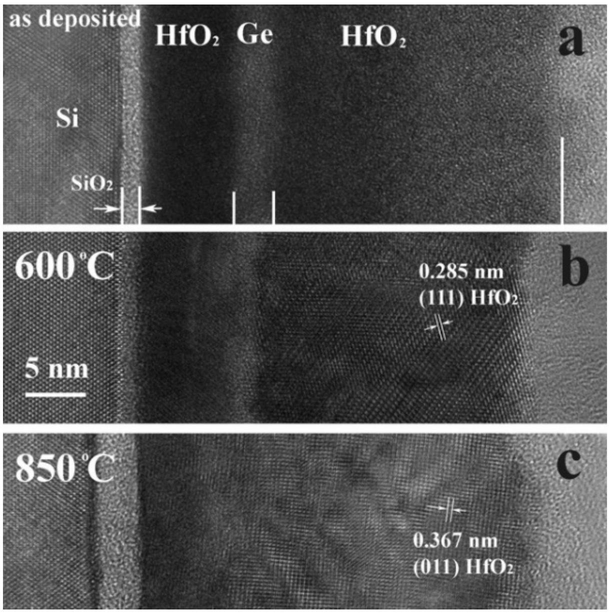

Fig.2.1. HRTEM images on A-MS sample for a) as-deposited, b) 600°C RTA and c) 850°C RTA [17].

Figure 2.2,a evidences Ge NPs in HAA.DF-STEM and HRTEM images measured on A-MS samples annealed at 600°C. The *Z*-contrast shows the presence of Ge NPs with diameters between 5 and 7 nm located in initial as-deposited position. From HRTEM images is impossible to evidence that Ge NPs are crystallized as cubic Ge and monoclinic HfO_2 have similar lattice constants [22]. The Raman spectra (Figure 2.2, b) show that Ge NPs are crystallized, in fact being Ge NCs. The experimental curve was modeled using Richter phonon quantum confinement model [23]. The experimental and theoretical curves are presented in Figure 2.2, b. From modeling, it results that Ge NCs in the intermediate layer have average diameter of 6.5 nm in good agreement with HAADF-STEM results.

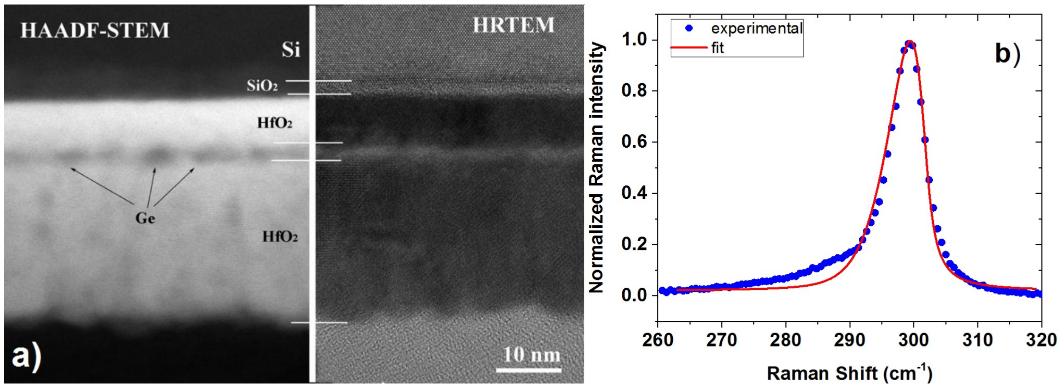

Fig.2.2. a) HAADF-STEM and HRTEM images and
b) Raman spectra – experimental and fit obtained on A-MS-600 sample [17].

Another confirmation of correct position of Ge NCs in trilayer capacitors comes from XPS analysis of A-MS-600 sample (Figure 2.3). The XPS measurements were taken at different depths from the free surface by using 2.5 nm sputtering steps.

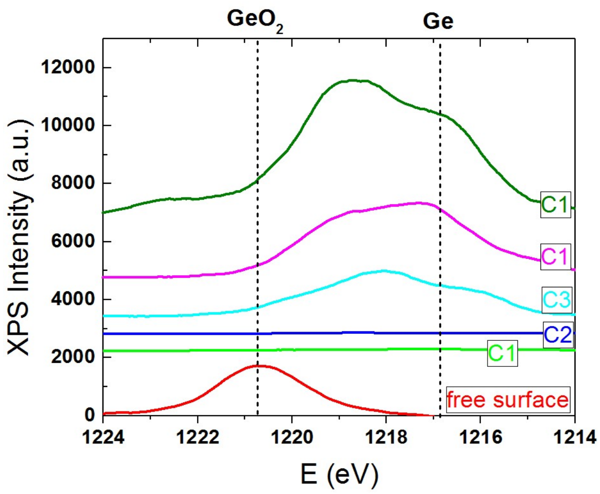

Fig. 2.3. XPS spectra of Ge 2p3/2 obtained on A-MS-600 sample [17].

In Figure 2.3 one can see that at the free surface a maximum in XPS curve (1220.6 eV) appears showing that Ge is oxidized [24]. By sputtering the trilayer at 2.5 nm and 5 nm (C1 and C2) under the free surface no Ge signal is recorded. The sputtering was performed with 2.5 nm steps in the depths. The Ge signal appears at the depth of 22.5 nm (C3) where C3 curve presents two maxima corresponding to metallic Ge (1217 eV) and oxidized Ge [24]. The intensity ratio of metallic Ge and oxidized one is 42/58. At 25 nm depth (C4) corresponding to the intermediate layer, the ratio increases to 60/40. By further sputtering the sample at 27.5 nm depth (C5) the ratio decreases at 44/56 meaning that the XPS curve is taken inside the intermediate layer but near the tunnel layer. The results obtained on XPS analysis prove that Ge NCs are located at the as-deposited position in trilayer.

Similar investigations of HAADF-STEM and HRTEM were made on EBE trilayers annealed at 850ºC (A-EBE-850) and 900 ºC (A-EBE-900) that are presented in Figure 2.4.

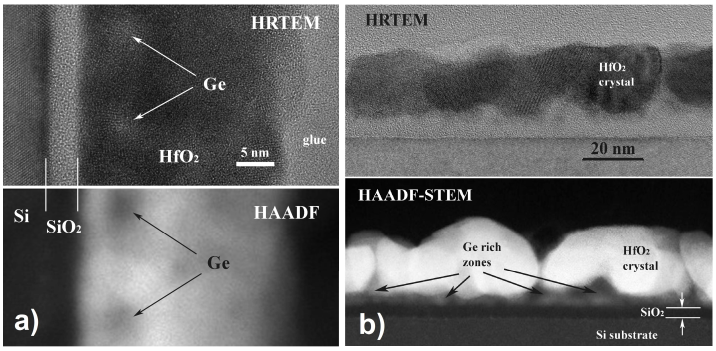

Fig. 2.4. HAADF-STEM and HRTEM images obtained on a)A-EBE-850 and b)A-EBE-900 [17].

One can observe that the sample A-EBE-850 contains Ge NPs with diameters of 5-6 nm similarly with A-MS-600 samples. In the samples A-EBE-900, Ge NPs (5-6 nm diameter) are located at the bottom part of the HfO_2 NCs layer. The Ge atoms that reach at the free surface either form GeO_2 or leave the sample.

The memory properties of the A samples were investigated by capacitance-voltage (*C-V*) and the retention time (*C-t*) measurements.

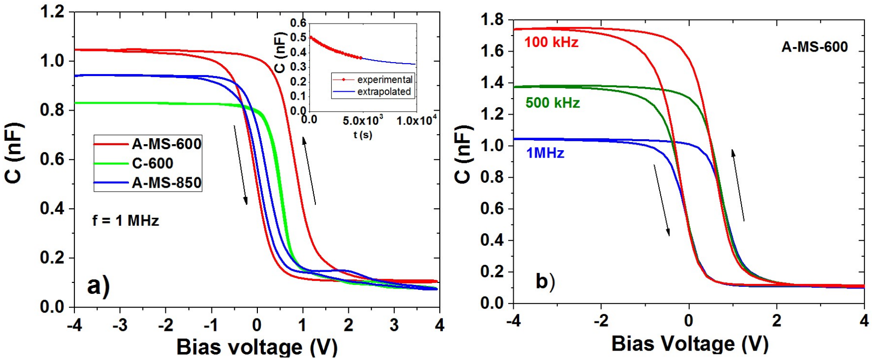

Fig.2.5. a) The C-V characteristics of the A-MS-600, A-MS-850 and C-600 sample; Inset: C-t characteristic b) C-V curves on A-MS-600 sample taken at 100 kHz, 500 kHz and 1MHz [17].

In Figure 2.5, *C-V* characteristics measured on A-MS-600, A-MS-850 and the control sample annealed at 600ºC (C-600) are shown. The C-V curves for A-MS-600 present hysteresis loops with counter-clockwise direction and a memory window of 1V. By increasing the annealing temperature at 850 ºC, the memory window decreases at 0.2V, that is supported by TEM images where no Ge NPs can be observed. The C-V curves taken on control sample C-600 without Ge show no hysteresis loop. In the inset of Figure 2.5, a is presented the *C-t* characteristics measured on A-MS-600, where the capacitance shows a decrease with 28% in the first 4000 s. In Figure 2.5b the *C-V* characteristics measured at different frequencies is presented. One can observe that the memory window is frequency independent which demonstrate that the hysteresis effect is given only by Ge NCs [25]. The memory characteristics measured on the A-EBE samples are presented in Figure 2.6. One can observe that the *C-V* characteristics is shifting to the negative voltages and the memory window decrease with increasing of the annealing temperature. The best memory window is obtained on the A-EBE-850 sample, the only contributors to the memory effect being the Ge NCs, similarly with the A-MS-600 sample.

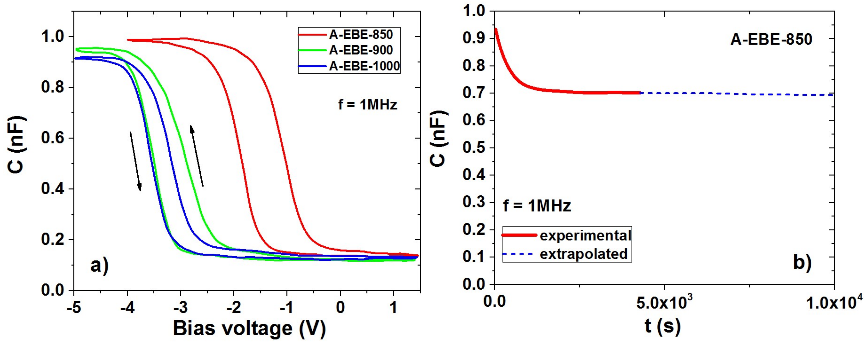

Fig.2.6. a) The C-V characteristics measured on the A-EBE samples annealed between 850 and 1000°C b) *C-t* characteristic obtained on A-EBE-850 sample [17].

The *C-t* curves show a decrease of capacitance value with 25% in the first 4000 s. The B-MS samples with the intermediate layer deposited by co-sputtering of Ge and HfO_2 that were annealed at 600 °C (B-MS-600) were also investigated by XTEM and HAADF-STEM (Figure 2.7) [26].

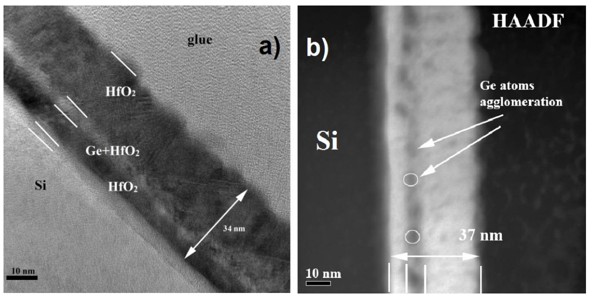

Fig. 2.7. a) XTEM and b) HAADF-STEM images taken on B-MS-600 sample [26].

From these images its results that inside the intermediate layer globular Ge atoms agglomeration are present. Similar to A-MS-600 sample, the tunneling and gate HfO_2 layers are crystallized. XPS analysis (Figure 2.8) taken on B-MS-600 sample shows similar results with that taken on A-MS-600 sample, but the XPS curve taken at 17.5 nm depth (C3) corresponding to intermediate layer is narrower and the intensity ratio of metallic Ge and oxidized Ge is 89/11. This means that the interfaces of intermediate layer with gate HfO_2 and tunnel HfO_2 are sharp and the density of Ge NCs is higher than in A-MS-600 trilayer.

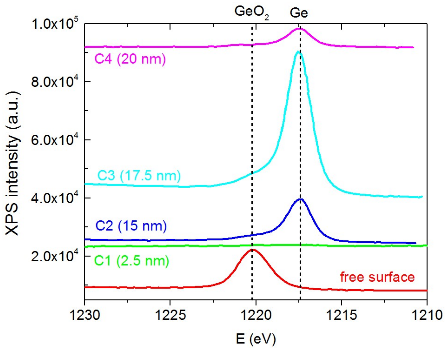

Fig. 2.8. XPS spectra of Ge 2p3/2 measured on B-MS-600 samples at free surface and different depths [26].

The memory properties of the B-MS-600 samples result from *C-V* at different frequencies and *C-t* curves shown in Figure 2.9.

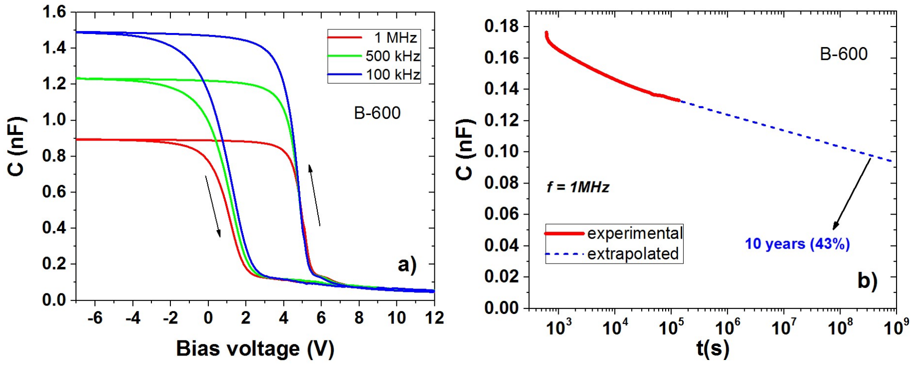

Fig. 2.9. a) *C-V* characteristics at different frequencies and b) *C-t* characteristics measured on B-MS-600 samples [26].

For B-MS-600 capacitors, *C-V* characteristics show a counter-clockwise hysteresis loop with 3.1 V memory window. The small shift of capacitance with frequency is due to the series resistance of interfaces inside capacitor (tunnel HfO_2/Si, tunnel layer/intermediate layer, intermediate layer/gate HfO_2) [27].

The charge retention measurements (*C-t*) show a capacitance decrease with 14% after 10^4 s, with the capacitance extrapolation to 43% at 10 years after [28].

3. Study of Ge nanoparticles embedded in TiO_2

In this section, electrical and photoelectrical properties of the Ge NPs embedded in TiO_2 are studied. For this, a Ge-TiO_2 layer with 60% Ge content and 180 nm thickness was deposited by co-MS of Ge and TiO_2 on SiO_2 (400 nm thickness) / n-type Si substrate. Then, the samples were annealed by RTA at 550°C for Ge NCs formation in TiO_2 matrix. For (photo)electrical measurements, Al coplanar electrodes were evaporated. In Figure 3.1 the structure analysis of Ge NCs in TiO_2 matrix is presented.

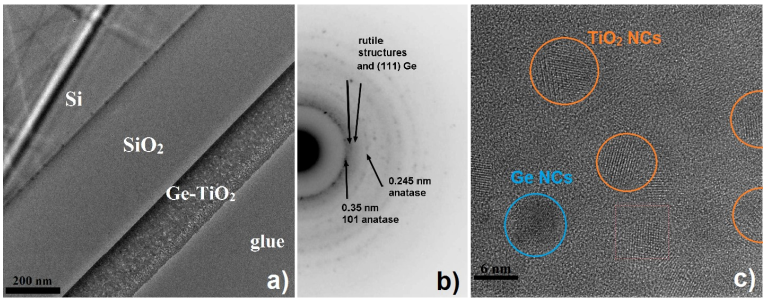

Fig. 3.1. a) XTEM, b) SAED and c) HRTEM images of the Ge-TiO_2 sample annealed at 550°C.

The XTEM image (Figure 3.1, a) shows the sample configuration of Ge NCs-TiO_2/SiO_2/Si. The SAED image (Figure 3.1, b) shows that the active Ge NCs-TiO_2 layer is crystallized with a dominant TiO_2 anatase phase (and some rutile traces) and cubic Ge (111) reflections that correspond to Ge NCs. The HRTEM image (Figure 3.1, c) also shows that the layer contains Ge and TiO_2 NCs with 4-6 nm diameter separated by amorphous matrix. The electrical properties of the active Ge-TiO_2 layer were investigated by dark current-voltage (*I-V*) (Figure 3.2, a) and current-temperature (*I-T*) measurements (Figure 3.2, b).

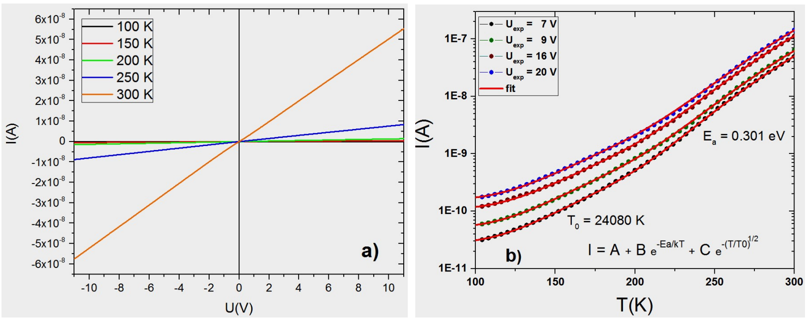

Fig. 3.2. Dark a) I-V at different temperatures and b) I-T characteristics at different voltages measured on the Ge-TiO_2 annealed at 550 °C.

The dark *I-V* curves are linear at all measurement temperatures between 100 and 300 K showing the good ohmic Al contacts with Ge NCs in TiO_2 layer. The *I-T* characteristics were modeled using two conduction mechanisms, namely thermally activated tunneling between Ge NCs at low temperatures, and thermal activation of carriers with an activation energy of 0.30 eV. The photoconduction properties of the Ge NCs in TiO_2 layer were studied by measuring of photocurrent spectra, $I_f - \lambda$, in the wavelength interval of 600÷1300 nm at different voltages (Figure 3.3). One can see that the spectra presents two maxima, one positioned at λ = 1100 nm, and the other one at λ = 870 nm. Depending on the bias voltage (U) the relative intensity of two maxima changes, so that at U < 12 V the maximum located at 1100 nm is dominant, while at U > 12 V the maximum at 870 nm becomes dominant. The maximum located at λ = 1100 nm (1.12 eV) is due to the surface photovoltage effect and thus corresponds to Si bandgap, while the maximum at 870 nm is due to Ge NCs.

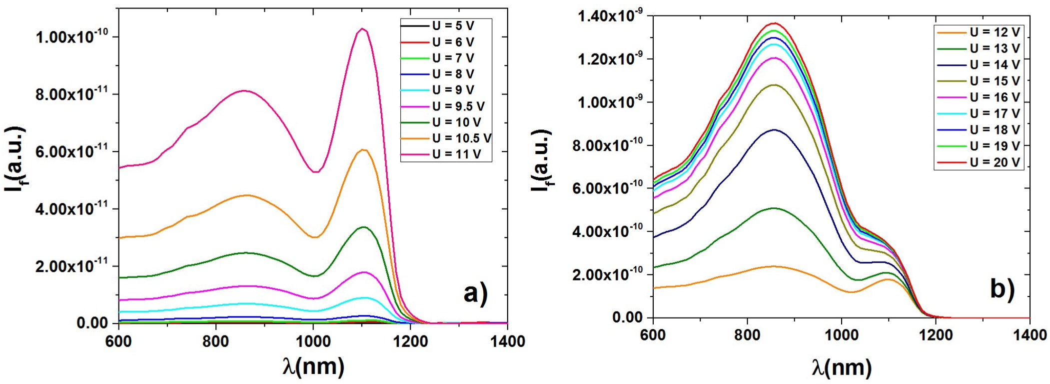

Fig. 3.3. Spectral distribution of the photocurent at a) low voltage and b) high voltage.

Conclusions

In the PhD. Thesis the memory and photoelectrical properties of Ge NCs embedded in HfO_2 and TiO_2 matrix, respectively were studied.

Regarding the system based on Ge NCs embedded in HfO_2, the best memory properties were obtained on the trilayer MOS-like capacitors prepared by magnetron sputtering and subsequent RTA at 600°C.

The memory effect is only due to Ge NCs embedded in HfO_2 matrix, positioned at a tunnelling distance from the Si substrate.

The A-MS-600 capacitors with initial as-deposited intermediate layer of continuous Ge have memory window of 1 V and good retention time characterized by a capacitance decrease with 28% in the first 4×10^3 s.

The B-MS-600 capacitors with initial co-deposited Ge-HfO_2 intermediate layer show much improved properties, i.e. 3.1 V memory window and a capacitance decrease with 14% in the first 10^4 s.

Concerning systems of Ge NCs embedded in TiO_2, we evidenced in the dark *I-T* characteristics two conduction mechanisms, namely thermally activated tunnelling between Ge NCs at low T and thermal activation of carriers at high T.

The spectral distribution of the photocurrent presents two main maxima, one positioned at λ = 870 nm corresponding to Ge NCs contribution and one at λ = 1100 nm corresponding to Si bandgap due to surface photovoltage assisted photoconductivity in Ge NCs -TiO_2 on SiO_2 (400 nm)/Si.

R E F E R E N C E S

[1] M. A. Smith *et al.*, Nat. Commun. **5**, 4506 (**2014**).

[2] I. Capan *et al.*, Beilstein J. Nanotechnol. **5**, 1787 (**2014**).

[3] C. P. Church *et al.*, Appl. Phys. Lett **103**, 223506 (**2013**).

[4] V. Mikhelashvili *et al.*, Appl. Phys. Lett **98**, 212902 (**2011**).

[5] J.-G. Lee *et al.*, Electron. Lett. **49**, 8 (**2013**).

[6] H. H. Nguyen *et al.*, J. Electrochem. Soc. **158**, 10 (**2011**).

[7] Y.-H. Wu *et al.*, IEEE Electron Device Lett. **31**, 9 (**2010**).

[8] Y.-H. Wu *et al.*, IEEE Electron Device Lett. **30**, 12 (**2009**).

[9] N. Miyata, Materials ***5**,* 512 (**2012).**

[10] C. Lee *et al.*, J. Vac. Sci. Technol. B **22**, (**2004**).

[11] C. S. Kang *et al.*, Appl. Phys. Lett. **81**, 14, (**2002**).

[12] H. Kamada *et al.*, Appl. Phys. Lett **93**, 212903 (**2008**).

[13] G. D. Wilk *et al.*, J. Appl. Phys. **87**, 484 (**2000**).

[14] X.-J. Liu *et al.*, Appl. Surf. Sci. **289**, 332 (**2014**).

[15] A. M. Smith and S. Nie, Accounts Chem. Res. **43**, 2 (**2010**).

[16] D. Vasilache *et al.*, Phys. Status Solidi A 213, 255-259 (**2016**).

[17] A. Slav *et al.*, Scripta Mater. **113**, 135–138 (**2016**).

[18] R. Bar *et al.*, Appl. Phys. Lett **107**, 093102 (**2015**).

[19] K. Ilse *et al.*, Phys. Status Solidi A **1**, 6 (**2016**).

[20] G. He, Z. Sun, *High-k Gate Dielectrics for CMOS Technology* (Wiley-VCH, Weinheim, Germany, **2012**).

[21] K. T. Jacob *et al.*, Int. J. Mater. Res. **98**, 776 (**2007**).

[22] C. Bonafos *et al.*, Mat. Sci. Semicon. Proc. **15**, 615 (**2012**).

[23] A.-M. Lepadatu *et al.*, J. Nanopart. Res. **15,** 1981 (**2013**).

[24] J.F. Moulder, W.F. Stickle, P.E. Sobol, K. Bomben, in: J. Chastain (Ed.), Handbook of X-ray Photoelectron Spectroscopy, 2nd ed. Perkin-Elmer Corporation (Physical Electronics), (**1992**).

[25] L. W. Teo *et al.*, Appl. Phys. Lett. **81**, 3639 (**2002**).

[26] A.M. Lepadatu *et al., Single layer of Ge quantum dots in HfO_2 for floating gate memory capacitors*, paper NANO-112847.R1 accepted for publication in Nanotechnology.

[27] B. Yao *et al.*, Appl. Phys. Lett. **100**, 222903 (**2012**).

[28] A. J. Hong *et al.*, J. Appl. Phys. **110**, 054504 (**2011**).